Delft University of Technology

QuadWave1D

An optimized quadratic formulation for spectral prediction of coastal waves

Akrish, Gal; Reniers, Ad; Zijlema, Marcel; Smit, Pieter

Important note
To cite this publication, please use the final published version (if applicable).
Please check the document version above.

QuadWave1D: An optimized quadratic formulation for spectral prediction of coastal waves

Gal Akrish [a,*], Ad Reniers [a], Marcel Zijlema [a], Pieter Smit [b]

[a] *Department of Hydraulic Engineering, Faculty of Civil Engineering and Geosciences, Delft University of Technology, The Netherlands*
[b] *Sofar Ocean, San Francisco, USA*

ARTICLE INFO

ABSTRACT

Spectral information of coastal waves and the associated statistical parameters (e.g., the significant wave height and mean wave period) over large spatial scales is essential for many applications (e.g., coastal safety assessments, coastal management and developments, etc.). This demand explains the necessity for accurate yet effective models. A well-known efficient modelling approach is the quadratic approach (often referred to as frequency-domain models, weakly nonlinear mild-slope models, amplitude models, etc.). The efficiency of this approach is achieved through modelling reduction of the original governing equations (e.g., Euler equations). Most significantly, wave nonlinearity is described solely by a single quadratic mode-coupling term. Therefore, doubts arise with regard to the predictive capabilities of the quadratic approach to reliably describe the nonlinear development of waves in the coastal environment where nonlinearity is typically significant. This study attempts to push the limit of the prediction capabilities of nonlinear coastal waves based on the quadratic approach. To this end, an optimization process is proposed, striving to extract the quadratic formulation which describes most adequately nonlinear wave developments over water depths and bathymetrical structures which characterize the coastal environment. The outcome is the model QuadWave1D: a fully dispersive quadratic model for coastal wave prediction in one-dimension. Based on a wide set of examples (including monochromatic, bichromatic and irregular wave conditions) and comparing to other representative quadratic formulations, it is found that QuadWave1D presents superior predictive capabilities of both the sea-swell components and the infragravity field.

1. Introduction

The prediction of coastal waves over large scales is crucial to coastal communities and municipalities, as they force nearshore circulation (e.g., Longuet-Higgins, 1970; Bowen, 1969; Ruessink et al., 2001 and Reniers and Battjes, 1997) and sediment transport processes (e.g., Van Rijn, 1993 and Fredsoe and Deigaard, 1992), as well as controlling shipping operations and associated downtime, and coastal safety through beach and dune erosion and potential inundation (e.g., Vellinga, 1982 and Roelvink et al., 2009).

Accurate determination of wave forcing in the coastal environment requires adequate description of shallow water nonlinearity. Time-domain models (e.g., Zijlema et al., 2011 and Shi et al., 2012) allow detailed and accurate modelling of nonlinear wave transformation, and therefore, enable to study the associated wave impacts nearshore (e.g., Roeber and Bricker, 2015). However, over coastal regions of large scales, this detailed wave prediction becomes impractical in terms of computational time. As a result, practitioners usually rely on wave data obtained using spectral models (e.g., SWAN model, Booij et al., 1999, WAVEWATCH model, Tolman, 1991). Despite the gain in efficiency, spectral modelling of shallow water nonlinearity is significantly limited. Apart from the constraints and parameterization applied to limit energy exchanges with higher harmonics (Eldeberky, 1996), energy transfer to the infragravity band is entirely excluded (spectral modelling of infragravity response has recently gained progress, see e.g., Reniers and Zijlema, 2022).

A well-known modelling alternative enabling practical (in terms of computational time) large scale wave prediction is the quadratic approach (often referred to as frequency-domain models, nonlinear mild-slope models, amplitude models, etc.). This modelling approach is less accurate than time-domain models, but allows for a more adequate and detailed description of shallow water nonlinearity compared to spectral models. The efficiency of this approach stems from a significant modelling reduction of the original governing equations (e.g., Euler equations). Most significantly, the description of wave nonlinearity

---

* Corresponding author.
 E-mail address: G.Akrish@tudelft.nl (G. Akrish).

essentially collapses into a single mode coupling term determined by the quadratic interaction coefficients. As a result, it is expected that the efficiency achieved by the quadratic approach is accompanied by a decrease in prediction accuracy. Minimizing the deterioration in model accuracy of the quadratic approach is at the centre of interest of this study.

Besides being a stand-alone model (Sheremet et al., 2016), the quadratic model is also the starting point for the spectral formulation of shallow water nonlinearity (e.g., Herbers and Burton, 1997). Therefore, the minimization of the error accompanied by the quadratic term, will not only lead to the improvement of the quadratic model itself, but will also enable a more reliable and accurate formulation of the nonlinear source term (i.e., the S_{nl3} formulation for shallow water nonlinearity) of spectral models (e.g., Booij et al., 1999).

The quadratic approach was initially formulated on the basis of time-domain weakly nonlinear Boussinesq models (e.g., Peregrine, 1967 and Madsen and Sørensen, 1992). Well known Boussinesq formulations were proposed by Freilich and Guza, 1984 and Madsen and Sørensen, 1993. Further developments of the quadratic approach were mainly devoted to the improvement of the linear wave description (i.e., dispersion relation and linear shoaling) and eventually led to the derivation of the so-called fully dispersive formulations (e.g., Agnon et al., 1993; Kaihatu and Kirby, 1995; Eldeberky and Madsen, 1999; Bredmose et al., 2005; Ardani and Kaihatu, 2019 and Kim and Kaihatu, 2021).

While there is no doubt that these developments have improved the linear properties of the quadratic model approach, there is doubt as to the improvement in the description of nonlinear evolution. This doubt stems from the fact that the improvement of the linear properties of the quadratic model is accompanied by a change in the quadratic coefficients, and therefore, also by a change in the truncation error obtained due to the modelling reduction associated with the formulation of the quadratic model. An indication for that is revealed through the examination of higher-order wave properties. Specifically, it seems that the existing fully dispersive formulations tend to overestimate the so-called amplitude dispersion over water depths that characterizes the coastal environment (e.g., Kaihatu, 2001; Bredmose et al., 2004, 2005 and Akrish et al., 2024). Not only does this cause the development of phase errors (Bredmose et al., 2005), it may also lead to unexpected evolution of energy spectra due to false impact of the modulational instability mechanism (Akrish et al., 2024). As a result, the evolution of both the primary wave field and the secondary components (i.e., the forced higher harmonics and infragravity band) may be predicted inadequately over coastal waters, despite the accurate implementation of linear wave properties.

This study aims to develop a new quadratic formulation that preserves full dispersion, but minimizes the error associated with the truncation in nonlinearity. In other words, this new formulation aims to optimize nonlinear model description based on the quadratic term, under the constraint of full linear dispersion. Instead of a rigorous physical-based formulation, the formulation proposed here is based on a parameterization which relies on available data. To start with, a general introduction of the quadratic modelling approach is presented in Section 2. Then, the general properties required to be satisfied by the quadratic coefficients are discussed in Section 3. These properties together with the requirement of full dispersion are used to constrain the search for the optimal quadratic formulation. The formulation itself is detailed in Section 4. Subsequently, a wide set of verification examples is considered in Section 5. These examples include monochromatic, bichromatic and irregular wave conditions. Through these examples, the predictive capabilities of the new formulation are demonstrated using comparisons to measured results, to the well verified SWASH model (Zijlema et al., 2011) and to other quadratic formulations. Finally, discussion and concluding remarks are drawn in Section 6.

2. The quadratic modelling approach

Generally speaking, the quadratic model derivation starts with an underlying time-domain model. The latter is usually written as a set of two equations for the surface elevation, η, and for the fluid velocity variable (may be the depth-averaged horizontal velocity or the horizontal velocity at a certain elevation level or the surface velocity potential etc.). Under the assumption of periodicity in time and slow modulation in space, the formulation can be written in terms of the spatially dependent complex amplitudes, a_n, defined by

$$\eta = \sum_n a_n \exp(-i\omega_n t), \tag{1}$$

where ω_n is the nth wave angular-frequency and t represents the temporal coordinate. The usual procedure to derive the quadratic formulation is through the multiple-scale method. A detailed account for such derivation can be found for instance in Dingemans (1997), Chapter 7 (see also Akrish et al., 2024, Appendix A). Ignoring medium variations, and assuming that the waves are long crested (e.g., confining the discussion to one spatial dimension), the resulted formulation describes a balance between the slow spatial variation of the amplitudes and the weak nonlinear quadratic term, written as

$$\partial_x a_n - ik_n a_n = -i \sum_r V_{r,n-r} a_r a_{n-r}, \tag{2}$$

where $V_{l,m}$ are the quadratic interaction coefficients, k_n is the nth wavenumber and x represents the spatial coordinate.

The prediction capabilities of different quadratic formulations are often initially evaluated based on their embedded linear dispersion, determined by k_n, and the second-order transfer function which is determined by both $V_{l,m}$ and k_n (e.g., Madsen and Sørensen, 1993; Eldeberky and Madsen, 1999; Bredmose et al., 2005 and Janssen, 2006). The latter defines the bound wave response and provides an indication for the predictive capabilities of weak nonlinearity, i.e., under the assumption that the so-called Ursell number, U_r, is relatively small. For small enough Ursell number ($U_r < 26$, using the definition given by Le Méhauté, 1976), the accuracy of the second order transfer function can be measured based on the second-order Stokes theory (expressions of which are given by, e.g., Hasselmann, 1962; Sharma and Dean, 1981 and Dalzell, 1999).

This preliminary assessment can also be used to classify the different quadratic formulations. At one end, the classical weakly dispersive Boussinesq formulation of Freilich and Guza (1984) is found. The other end can be defined by the fully dispersive model of Bredmose et al. (2005) which considers all possible second-order terms, and therefore, allows exact second-order transfer (i.e., the bound wave solutions according to this model match exactly to the solutions according to Stokes theory). The range of formulations placed in between consists of Boussinesq formulations with improved dispersion and fully dispersive formulations with different transfer function definitions. A well-known representation of the former is the formulation of Madsen and Sørensen (1993) which also serves as the starting point for the formulation of phase-averaged shallow water nonlinearity (Eldeberky, 1996) implemented in operational wave models (e.g., the SWAN model, Booij et al., 1999), while representation of the latter can be the well-known model of Kaihatu and Kirby (1995). Note that this model range also includes more advanced generalizations of the fully dispersive approach, such as the model by Eldeberky and Madsen (1999) and the model by Ardani and Kaihatu (2019). On the other hand, the model range excludes models which deviate from the structure defined in (2). Thus, for example, recent model generalization by Kim and Kaihatu (2021), which includes quadratic terms involving amplitude gradients (i.e., terms such as $a_r \partial_x a_{n-r}$), is outside the scope of the present investigation.

Over coastal waters, both linear dispersion and nonlinear wave–wave interaction are important. Specifically, it is essential that these processes are accurately described for adequate representation of the

balance between them and, e.g., the associated wave transformation towards breaking. Therefore, it is expected that the model by Bredmose et al. (2005), which exhibits accurate linear and nonlinear properties, will predict most adequately the evolution of coastal waves. However, a recent study by Akrish et al. (2024) shows otherwise. Particularly, the evolution of coastal waves was found to be largely determined by the amplitude dispersion, which is a nonlinear property that arises at third-order. Moreover, Akrish et al. (2024) showed that the tendency of fully dispersive models to overestimate the amplitude dispersion results in unfavourable modifications of the modulational instability mechanism (see a qualitative description by Lighthill, 2001, page 462, of the effect of amplitude dispersion on the development of a nonlinear modulated wave field leading to the emergence of the mechanism known as modulational instability). Consequently, these models may become modulationally unstable over much shallower water than expected and may be subjected to much stronger growth rates and much larger modulation ranges. As a result, predictions of coastal waves using fully dispersive models can be characterized by unexpectedly strong modulations of the sea-swell components and associated unexpected infragravity response. These results imply the impact of inadequate representation of wave properties at higher-order, and more generally, the consequences of the truncation in nonlinearity associated with the formulation of the quadratic approach.

To conclude, the indication provided by the second-order transfer function as to model prediction of nonlinearity seems to be inadequate. At least qualitatively, model prediction of nonlinearity can be said to be determined by the balance between wave interactions transferring energy towards super and sub harmonics. This nonlinear balance seems to be dependent on both the interaction coefficients, $V_{l,m}$, and the dispersion relation defined by k_n. It is hypothesized that under the constraint of full linear dispersion, there exist $V_{l,m}$ which optimize this nonlinear balance, leading to superior predictive capabilities of both the sea-swell components and the infragravity field over coastal waters. This study attempts to find these $V_{l,m}$. In addition to full linear dispersion, the search for the optimal $V_{l,m}$ is also constrained by general properties required for any candidate of $V_{l,m}$. These general properties are detailed next.

3. General properties for the quadratic interaction coefficients

The properties required to be satisfied by the quadratic interaction coefficients are explained in the following. The starting point is the definition of η based on the Fourier series in (1). Following this starting point, the reality of η yields the condition

$$(a_n)^* = a_{-n} \tag{3}$$

Based on this condition and assuming that k_n and $V_{l,m}$ are defined as real functions, the general quadratic formulation (2) leads to the following properties:

$$\begin{cases} k_{-n} = -k_n \\ V_{-l,-m} = -V_{l,m} \end{cases} \tag{4}$$

Without loss of generality, it will be convenient to assume the following symmetry:

$$V_{l,m} = V_{m,l} \tag{5}$$

This symmetry indeed holds for all the quadratic formulations discussed in Section 2 (see details in Akrish et al., 2024, Supplementary material). As a consequence of the properties defined by (4) and (5), the following result is obtained:

$$V_{l,-l} = -V_{l,-l} = 0 \tag{6}$$

An additional property is obtained through the analysis of the dynamical behaviour of a typical triad interaction of the quadratic system. To

this end, consider the following triad model:

$$\begin{cases} \partial_x a_1 - ik_1 a_1 = -i2V_{3,-2} a_3 a_{-2} \\ \partial_x a_2 - ik_2 a_2 = -i2V_{3,-1} a_3 a_{-1} \\ \partial_x a_3 - ik_3 a_3 = -i2V_{1,2} a_1 a_2 \end{cases} \tag{7}$$

This model is derived based on the quadratic model (2), by restricting the dynamics to three frequencies which satisfy the relation $\omega_1 + \omega_2 = \omega_3$. The corresponding coupled equations for the variance spectrum, $E_j = a_j a_{-j}$, are given by

$$\begin{cases} \partial_x E_1 = 4V_{3,-2} \text{Im}\{a_3 a_{-2} a_{-1}\} \\ \partial_x E_2 = 4V_{3,-1} \text{Im}\{a_3 a_{-2} a_{-1}\} \\ \partial_x E_3 = -4V_{1,2} \text{Im}\{a_3 a_{-2} a_{-1}\} \end{cases} \tag{8}$$

This system leads to the following Manley–Rowe relations (e.g., Craik, 1985):

$$\partial_x \left(\frac{E_1}{V_{3,-2}} + \frac{E_3}{V_{1,2}} \right) = 0, \quad \partial_x \left(\frac{E_2}{V_{3,-1}} + \frac{E_3}{V_{1,2}} \right) = 0, \quad \partial_x \left(\frac{E_2}{V_{3,-1}} - \frac{E_1}{V_{3,-2}} \right) = 0 \tag{9}$$

As is clearly described by these relations, the evolution of the variance spectrum is bounded if the quadratic coefficients $V_{1,2}$, $V_{3,-1}$ and $V_{3,-2}$ have the same sign. In that case, the wave components are periodically exchanging energy (energy loss by a_1 and a_2 is gained by a_3 and vice versa). Therefore, each variance component, E_j, is spatially oscillating, which implies on a conservative interaction (see further details by Craik, 1985 and Vanneste, 2005). This leads to the general conclusion that in order to obtain a quadratic formulation that is characterized by conservative and bounded triad interactions, its super and sub interaction coefficients should have the same sign, namely,

$$sgn\{V_{l,m}\} = sgn\{V_{l,-m}\} \tag{10}$$

for which

$$sgn\{l+m\} = sgn\{l-m\} \tag{11}$$

Finally, an additional property is obtained by requiring that the solutions for the bound super and sub harmonics be in phase and 180° out of phase with respect to the primary forcing, respectively. This requirement means that the second-order transfer function, $G_{l,m}$, which determines the bound solutions through the relation $G_{l,m} = V_{l,m}/(k_n - k_l + k_m)$, should obey to the following:

$$\begin{cases} G_{l,m} > 0, & sgn\{l\} = sgn\{m\} \\ G_{l,m} < 0, & sgn\{l\} = -sgn\{m\} \end{cases} \tag{12}$$

which also means that $V_{l,m} > 0$ for $l + m > 0$.

4. A parametric derivation of improved fully dispersive quadratic model

Generally speaking, there are an infinite number of fully dispersive formulations that can be defined, which satisfy the general properties of $V_{l,m}$ as defined above. Nevertheless, it is attempted here to find the $V_{l,m}$ that optimize prediction capabilities of nonlinear wave evolution. Since the interest here is devoted to the dynamics of coastal waves, the search is for $V_{l,m}$ with optimal performance over water depths that roughly satisfy $\mu \leq 2$, where $\mu = k_p h$ is the so-called depth parameter, k_p is the characteristic wavenumber of a considered wave field and h represents the water depth.

In contrast to the conventional rigorous formulation approach, the search for the optimal $V_{l,m}$ is performed here through an alternative approach using data of laboratory experiments and the well-validated time-domain model SWASH. Such an approach requires an ensemble of wave simulations which were conducted under the desired depth conditions and which describe spatially evolving and stationary (time-periodic) wave fields. For each such simulation, it is required to extract

the corresponding complex-amplitude vector and its spatial derivative at several different locations in order to construct an algebraic system which can be solved for $V_{l,m}$ (alternatively, it is also possible to construct similar system based on the energy-flux gradients and the bispectrum). This complex process requires large data sets with different conditions and requires to correctly evaluate numerical derivatives which pose difficulties due to the presence of noise. An additional difficulty arises as a result of the dependence of the extracted $V_{l,m}$ values on the amplitudes themselves, suggesting different values of $V_{l,m}$ for simulations of different Ursell numbers. Given the complexity of this direct method, an alternative procedure is proposed here. This procedure would not lead to the ambitious goal of finding the optimal values of $V_{l,m}$, but may allow formulating a satisfactory and robust solution for $V_{l,m}$, which avoids the dependence on the amplitudes.

The alternative procedure proposed here relies on a weight function, $W_{l,m}$, that is defined through a basic parameter χ and through three additional parameters, α_1, α_2 and α_3 as follows:

$$W_{l,m} = \exp\left[-\left(\frac{\chi}{\alpha_3}\right)^{\alpha_2}\right] \qquad (13)$$

where χ is defined as

$$\chi = |k_{lm}|h\left(\frac{|k_{lm}|}{|k_n|}\right)^{\alpha_1} \qquad (14)$$

and where α_1, α_2 and α_3 define ranges of positive numbers over which the optimization is performed. Finally, k_{lm} is defined as $k_{lm} = k_l + k_m$. The weight function given by (13) together with the quadratic coefficients suggested by Bredmose et al. (2005) are used to define the following weighed coefficients:

$$V_{l,m}^{WQC} = W_{l,m} V_{l,m}^{BC} \qquad (15)$$

where the superscripts WQC and BC stand for 'Weighted Quadratic Coefficients' and 'Bredmose Coefficients', respectively (for convenience, the definition for $V_{l,m}^{BC}$ is included in Appendix A). Thus, instead of finding many discrete optimal values of $V_{l,m}$ directly, the optimization problem proposed here amounts to finding only three values of α_1, α_2 and α_3 which minimize the prediction errors with respect to data of laboratory experiments and SWASH. It remains to explain the selected functional structure of the weight function (which is also defined by χ) and the choice to use $V_{l,m}^{BC}$.

The chosen definition of $W_{l,m}$ is based on the following requirements. First, it should be defined such that $V_{l,m}^{WQC}$ complies with the general properties detailed in Section 3. Second, it is proposed here that $W_{l,m}$ would converge to zero as μ increases. The motivation behind this second requirement is to prevent overestimation of the amplitude dispersion and the associated modifications of the modulational instability mechanism over coastal waters (see discussion in Section 2 and Akrish et al., 2024). In addition, forcing $W_{l,m}$ to converge to zero for high μ values also aims to avoid other unfavourable nonlinear mechanisms which seem to characterize models with full dispersion and which lead to an unwanted dependence on the choice of the maximum frequency (see Section 4.2). However, attenuating the interaction coefficients would also result in unfavourable consequences. Specifically, this constraint would lead to inaccurate predictive capabilities of the second-order bound waves in deep to intermediate waters. To conclude, this second requirement essentially sacrifices the accuracy of the bound wave response in deep to intermediate waters in favour of adequate wave evolution in intermediate to shallow waters.

The definition of $W_{l,m}$ as given by (13) satisfies the first requirement due to its symmetry with respect to the indices l and m and since it is positive. The second requirement is satisfied as well under the condition that χ is positive and represents in a certain way the parameter μ. The selected exponential structure of $W_{l,m}$ indeed preserves weighted regions that correspond to interactions of waves over relatively shallow waters and weakens weighted regions that correspond to interactions in deep water.

Table 1
Physical parameters of the examples considered for the optimization process.

Example	L (m)	h (m)	T (s)	μ	amp_I (m)	U_r
E1	40	0.4	3.3	0.39	0.03	38
E2	25	0.4	2.5	0.53	0.042	29
E3	10	0.4	2	0.68	0.06	26

The specific definition of χ, as given by (14), is intimately related to the quadratic interaction coefficients of Freilich and Guza (1984) (see Freilich and Guza, 1984, Eqs. 16a and 16b). The implementation of this definition in $W_{l,m}$ generates a structure which roughly describes straight contour lines with a 45° decreasing slope for the superharmonic interactions and a −45° decreasing slope for the subharmonic interactions (see Fig. 1). This is more or less the structure of the normalized coefficients and transfer function of Freilich and Guza (1984) (see Janssen, 2006, Fig. 3.6 and Akrish et al., 2024, Fig. 1). Thus, the weighted coefficients, $V_{l,m}^{WQC}$, defined through the functional structure of $W_{l,m}$, the definition of χ and the coefficients of Bredmose et al. (2005) presents a structure similar to that of Freilich and Guza (1984). This choice is motivated by the success of the quadratic coefficients of Freilich and Guza (1984) to accurately describe energy exchanges over shallow waters (e.g., Herbers et al., 2000; De Bakker et al., 2015 and Rijnsdorp et al., 2022). Based on this motivation one may argue that the quadratic coefficients of Freilich and Guza (1984) could be used directly. However, following the experience of the present investigation, direct use of the coefficients of Freilich and Guza (1984) under fully dispersive conditions would not yield satisfactory results.

At this stage, the roles of α_1, α_2 and α_3 are introduced. The parameter α_1 allows for some structural deviations of the contour lines including their rotation (see the different contour pattern obtained for different values of α_1 in Fig. 1). The parameters α_2 and α_3 determine the dispersion (similar to the definition of the standard deviation) and the steepness (namely, how fast is the transition from 1 to 0) of the contours, respectively. Different values of α_1, α_2 and α_3 generate different contour patterns of $V_{l,m}^{WQC}$, resulting in different dynamical balance of superharmonics and subharmonics energy transfers. Finally, note that the allowable ranges for α_1, α_2 and α_3 are limited, so that only reasonable candidates of $V_{l,m}^{WQC}$ are included as part of the optimization. For example, to guarantee the convergence of $V_{l,m}^{WQC}$ to zero for deep water interactions, it is required that $\alpha_1 > 0$ (see Fig. 1). Additionally, to allow for a reliable subharmonic bound wave forcing, α_1 should also subjected to an upper bound limit of around 2 (refer again to Fig. 1). Similarly, the values for α_2 and α_3 are limited as well to exclude exceptional and undesirable candidates of $V_{l,m}^{WQC}$.

4.1. The optimization process

The optimization process is summarized by the following. In total, data of three examples of monochromatic wave propagation along a flume of constant depth are considered. These examples are referred to as E1, E2, and E3. The physical parameters that define each of the examples are summarized in Table 1. These include the length of the flume L, the water depth h, the wave period T, the depth parameter μ, the incoming wave amplitude amp_I and the Ursell parameter U_r.

These examples were chosen such that the nonlinearity of the generated monochromatic wave is relatively weak (all the examples assigned to similar small U_r values to avoid wave breaking). Additionally, the depth parameters of the examples were selected such that a wide range sample of $V_{l,m}^{WQC}$ values is generated. Specifically, the sample should be concentrated over $(k_l h, k_m h)$ region that corresponds to coastal water depths. The effective sample of $V_{l,m}^{WQC}$ values over $(k_l h, k_m h)$ (including points that correspond to interactions of up to $O(\epsilon^4)$) is described in Fig. 1. These points include $V_{l,m}^{WQC}$ values that correspond to the $O(\epsilon^2)$ self interaction of the first harmonic, the $O(\epsilon^3)$ super and sub interactions between the first and the second harmonics, the $O(\epsilon^4)$
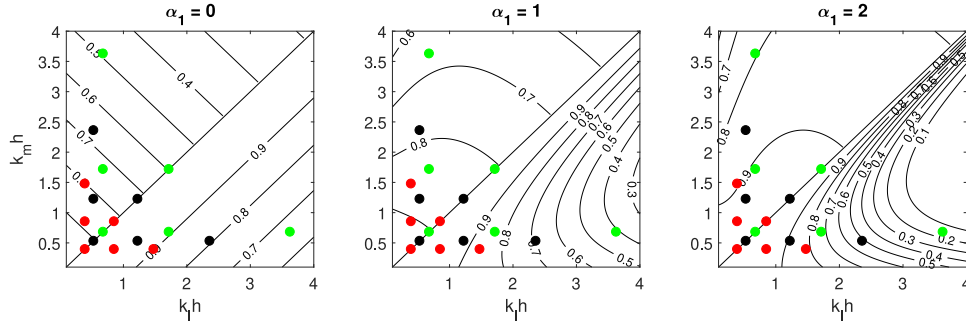
Fig. 1. The weighted quadratic coefficients, $V_{l,m}^{WQC}$, normalized by the quadratic coefficients of Bredmose et al. (2005) (or simply the weight function $W_{l,m}$) for three values of α_1 and using the parameter values $\alpha_2 = 1.4$ and $\alpha_3 = 5.5$. Self interaction coefficients are presented along the main diagonal of each panel, while super and sub interaction coefficients are presented by the upper and lower triangular of each panel, respectively. The dots represent the sampled interaction coefficients that correspond to interactions of up to $O(\epsilon^4)$ due to the different considered examples. Red, black and green dots correspond to E1, E2, and E3 respectively.

self interaction of the second harmonic and the $O(\epsilon^4)$ super and sub interactions between the first and the third harmonics.

Based on the above described examples (E1, E2, and E3), the optimization process strives to find the weighted quadratic formulation (using the full linear dispersion relation and $V_{l,m}^{WQC}$) which minimizes the prediction errors (defined by (17)) with respect to given data. The search is performed over the following domain:

$$\begin{cases} \alpha_1 = [0.5, 2] \\ \alpha_2 = [1, 2] \\ \alpha_2 = [2, 10] \end{cases} \tag{16}$$

The accuracy of the results at each point $(\alpha_1, \alpha_2, \alpha_3)$ is examined with respect to experimental data and results of simulation using SWASH. To this end, the following normalized error is defined:

$$e(\alpha_1, \alpha_2, \alpha_3) = \sum_j \sum_i |amp_{i,j} - amp_{R,i,j}|/amp_I \tag{17}$$

where j runs over the first three harmonics and i runs over the data locations. The reference amplitudes, $amp_{R,i,j}$, are based on SWASH results for E1 and E3, and on the experimental results of Chapalain et al. (1992) for E2. The results through SWASH are obtained using two vertical layers, spatial step of $\Delta x = 0.01$ m, time step of $\Delta t = 0.0025$ s and simulation time of 10 min. The results of the quadratic model are computed based on the RK4 method, using the first six harmonics only (the first harmonic also serves as the frequency step and the maximum frequency is the sixth harmonic) and a spatial step of $\Delta x = 0.05$ m. Finally, the normalized errors obtained through each of the examples are summed together, providing the point which scores the minimum total normalized error with respect to the reference data. This point is given by $(\alpha_1 = 1, \alpha_2 = 1.4, \alpha_3 = 5.5)$, as partially described (over (α_2, α_3) only) by Fig. 2.

4.2. Nonlinear properties and model sensitivity to the presence of high frequencies

The quadratic model with the optimized weighted quadratic coefficients is referred to as the QuadWave1D model (see detailed formulation of its quadratic coefficients in Appendix A). The nonlinear properties of QuadWave1D are investigated here through comparisons to the properties of other representative quadratic formulations. In accordance with the classification described in Section 2, the selected representative quadratic formulations are the weakly dispersive Boussinesq formulation of Freilich and Guza (1984), the Boussinesq formulations with improved dispersion of Madsen and Sørensen (1993) and Nwogu (1993) and the fully dispersive formulations by Kaihatu and Kirby (1995) and Bredmose et al. (2005). Note that Nwogu (1993) actually presents a time-domain model formulation. Here though, this
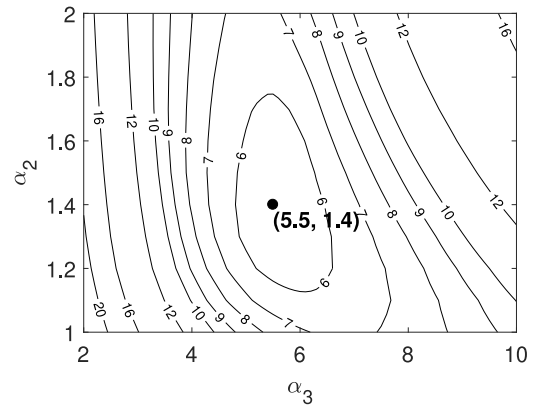

Fig. 2. Normalized total amplitude error with respect to experimental data following Chapalain et al. (1992) and results of simulation using SWASH for $\alpha_1 = 1$.

reference is used to refer to the corresponding quadratic formulation. The derivation of Nwogu's quadratic formulation and the formulations of the other quadratic models are summarized in Akrish et al. (2024), Supplementary material.

At first, the bound wave solutions normalized by the solutions due to the second-order Stokes theory are considered. The normalized bound solutions due to QuadWave1D are actually given by the weight function $W_{l,m}$, illustrated by the middle panel of Fig. 1. This is understood by recalling that QuadWave1D is fully dispersive and its quadratic coefficients are defined based on $V_{l,m}^{BC}$ which lead to exact second-order transfer. Therefore, the normalization with respect to the solutions of the second-order Stokes theory becomes equivalent to the normalization of $V_{l,m}^{WQC}$ with respect to $V_{l,m}^{BC}$, which equals to $W_{l,m}$. The normalized bound solutions of QuadWave1D can be compared to the normalized bound solutions of the other quadratic formulations which are provided by Akrish et al. (2024), Fig. 1. Clearly, QuadWave1D underpredicts bound wave responses. Insignificant deviations appear for interactions within the radius $\mu < 2$, while significant underestimation arises if one of the forcing waves corresponds to $\mu > 2$.

In addition, the amplitude dispersion due to self interaction, $\omega_{p,p}^{(2)}$, and the modulational instability threshold are examined. These third-order properties are calculated as functions of the interaction coefficients and the dispersion relation using expressions given by Akrish et al. (2024) (see Akrish et al., 2024, Eqs. 14–15 and Eq. 25). The results are shown in Fig. 3. These results are based on the different quadratic formulations considered here and are compared to well-known analytical results at third-order (see, e.g., Whitham, 1974, Section 16 and Mei et al., 2005, Section 13).
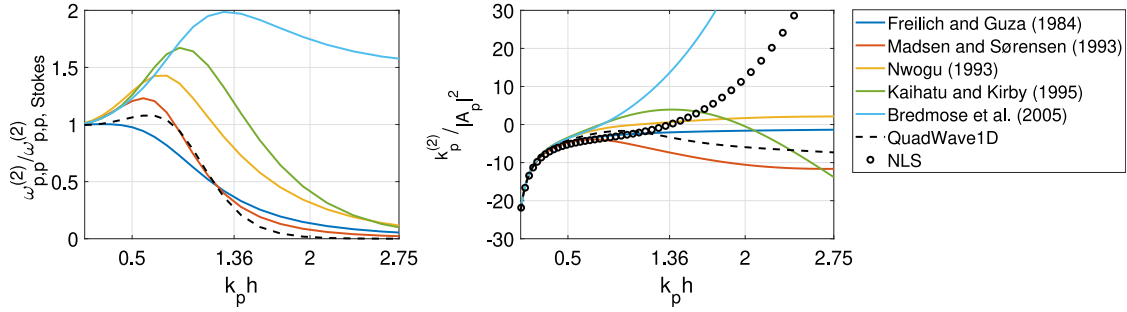
Fig. 3. Normalized amplitude dispersion due self interactions (left panel) and modulationally stable/unstable regions (right panel).

All the considered quadratic formulations show deviations of amplitude dispersion with respect to third-order Stokes theory (represented by $\omega_{p,p,Stokes}^{(2)}$). QuadWave1D and the Boussinesq formulations appear to be more consistent with Stokes theory for $\mu < 1$. However, for deep waters, these models demonstrate considerable underestimation of amplitude dispersion effects, indicating significant phase errors in wave prediction (see, e.g., recent demonstration by Stuhlmeier and Stiassnie, 2021, Figs. 3 and 8, for the added value of the amplitude dispersion for predicting waves in deep water). The fully dispersive models tend to strongly overestimate the contributions of the amplitude dispersion. Apart from phase errors, this significant overestimation also leads to significant impact of the modulational instability mechanism over regions of μ where this mechanism is expected to be weak or absent (see further details in Akrish et al., 2024). The modifications in the modulational instability threshold are demonstrated by the right panel in Fig. 3 through comparison to third-order results provided by the nonlinear Schrödinger (NLS) equation. The instability threshold is described using the wavenumber correction due to self interaction, $k_p^{(2)}$, which accounts for the stabilizing effect of the wave-induced current (see discussion by Akrish et al., 2024, section 2.3.1). Instability is expected over $k_p h$ values for which $k_p^{(2)}/|A_p|^2 > 0$, where $|A_p|^2$ is the magnitude square of the carrier wave amplitude. As for the models of Freilich and Guza (1984) and Madsen and Sørensen (1993), QuadWave1D is shown to be modulationally stable and is therefore not exposed to false impact of modulational instability over coastal waters. However, as suggested by its deviations at second and third orders, QuadWave1D is not suitable for modelling of nonlinear waves under deep water conditions.

Returning now to examples E1, E2, and E3. Note that the satisfying performance of QuadWave1D for these examples has only been demonstrated so far based on the normalized error $e(\alpha_1, \alpha_2, \alpha_3)$, but has not been explicitly shown. An explicit presentation of this performance is provided by Figs. 4–6.

The results presented by Figs. 4–6 suggest that QuadWave1D adequately predicts the wave evolution in all of the three monochromatic examples considered. The adequate prediction is measured here on the basis of the magnitude of the amplitudes and the recurrence length, given by the beating pattern of the harmonics. The comparison between the quadratic formulations shows that QuadWave1D and the model by Nwogu (1993) present the most satisfying agreement with the data. The least favourable results are demonstrated by Kaihatu and Kirby (1995) and Bredmose et al. (2005). The deviations presented by these results are attributed to inadequate dynamical balance between the super and sub interactions which is controlled by the structure of $V_{l,m}$ and in particular by its degree of attenuation for increasing values of μ. This implies a dependence of the prediction of these models on the maximum considered frequency. To demonstrate this dependence, Fig. 7 shows model predictions for the case E2 due to Kaihatu and Kirby (1995) and Bredmose et al. (2005) and QuadWave1D, and for two maximum frequency values. Besides the unfavourable maximum frequency dependence of the models by Kaihatu and Kirby (1995) and Bredmose

et al. (2005), the results of Fig. 7 also suggests the insensitivity of QuadWave1D to the maximum frequency. The observed dependence of model prediction on the maximum considered frequency (which satisfies the frequency limit due to numerical stability), constitutes a serious modelling problem. Such a problem requires further analysis which is beyond the scope of the present study.

Finally, the satisfying agreements presented by QuadWave1D should not provide a firm conclusion regarding its overall performance. The judgment concerning the predictive capabilities of QuadWave1D should rather be determined on the basis of independent cases, which are considered next.

5. Model verification

The prediction capabilities of QuadWave1D are studied here through comparisons with different laboratory experiments and comparing to the predictions of the representative quadratic formulations introduced in Section 4. For some examples, results due to the SWASH model are included as an additional reference. The presented verification considers first two basic monochromatic cases, and later on, also more general cases where the incoming wave field is either bichromatic or described through a continuous spectrum.

Since most of the examples presented here involve bathymetry changes, the quadratic formulation (2) discussed so far should be modified to include the effect of wave shoaling. This can be readily implemented by using the energy-flux related amplitude, $b_n = a_n \sqrt{C_{g,n}}$ (see details in Akrish et al., 2024, Appendix A, also regarding the definition of $C_{g,n}$ for each of the considered quadratic formulations). Therefore, the modified quadratic formulation reads

$$\partial_x b_n - i k_n b_n = -i \sum_r \sqrt{\frac{C_{g,n}}{C_{g,r} C_{g,n-r}}} V_{r,n-r} b_r b_{n-r} \qquad (18)$$

The quadratic model (18) is solved numerically using the RK4 method. For most of the considered examples, the spatial step being used is $\Delta x = 0.05$ m (the exception is the monochromatic case in Section 5.1.2 for which $\Delta x = 0.025$ m), while the spectral resolution and thus also the number of realizations are determined for each example specifically. Similarly, all the computations with SWASH are performed here using two vertical layers, a spatial step of $\Delta x = 0.02$ m and a time step of $\Delta t = 0.005$ s, while the simulation time is determined separately for each example.

5.1. Monochromatic wave evolution

The predictive capabilities of QuadWave1D are first tested through two monochromatic examples. The first example is given by the 'Trial D' experiment conducted by Chapalain et al. (1992). This experiment describes the evolution of a progressive monochromatic wave in a flume of constant depth (see schematic illustration in Fig. 8). The incoming wave generated by the wavemaker is characterized by a relatively large U_r (see Table 2), implying strong nonlinear effects. Such
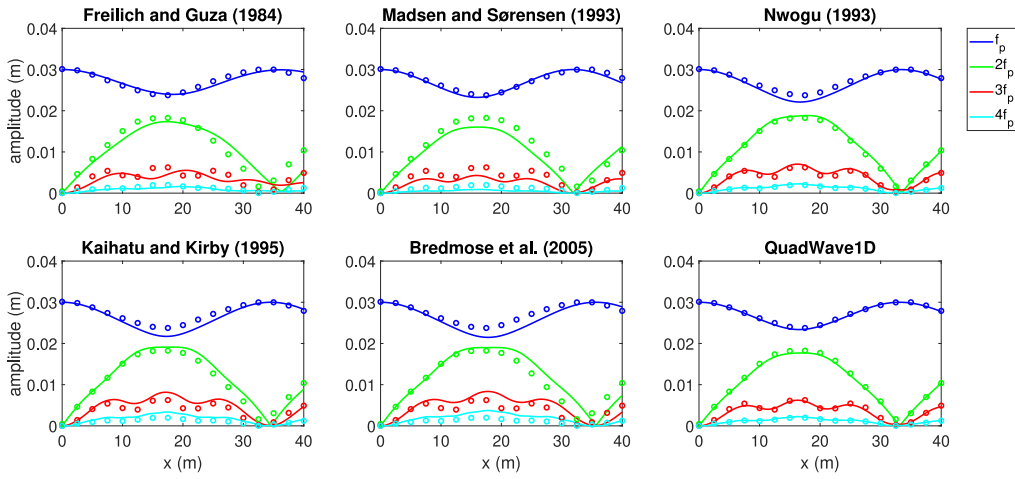
Fig. 4. Amplitude evolution of the first four harmonics as obtained by the different quadratic formulations (lines) and the SWASH model (circles) for example E1.

Fig. 5. Amplitude evolution of the first four harmonics as obtained by the different quadratic formulations (lines) and the laboratory results measured by Chapalain et al. (1992) (circles) for example E2.

Fig. 6. Amplitude evolution of the first four harmonics as obtained by the different quadratic formulations (lines) and the SWASH model (circles) for example E3.
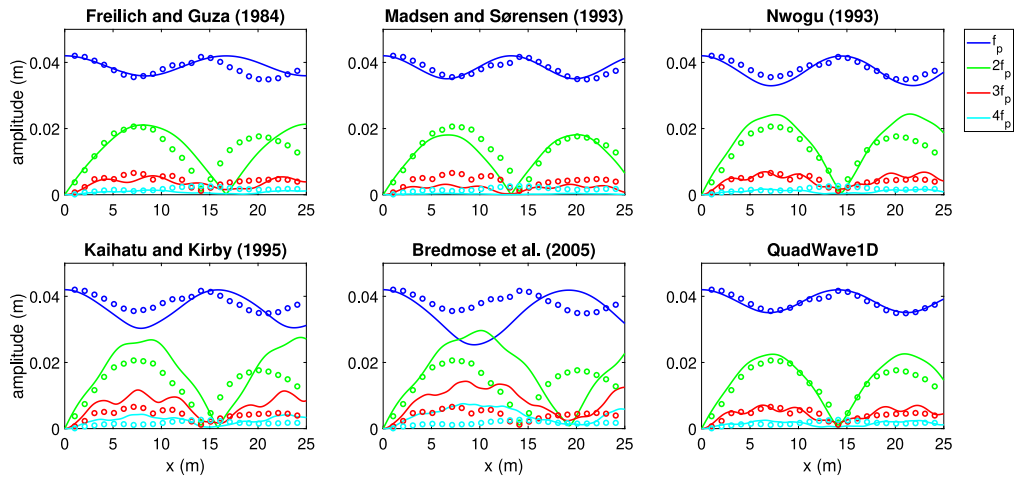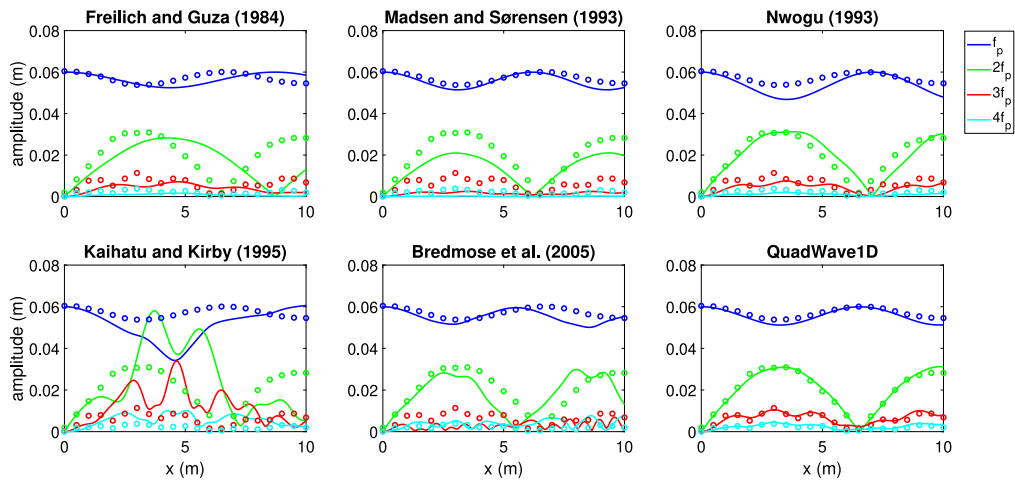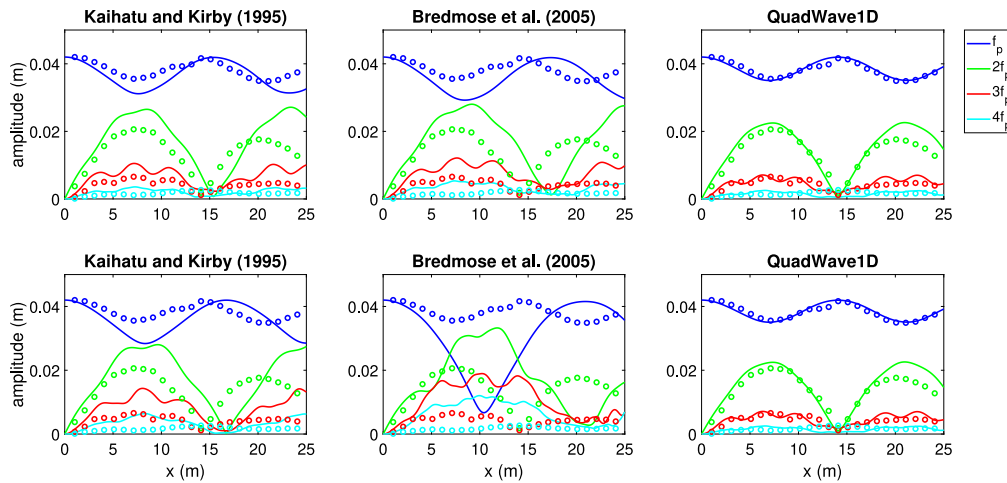
Fig. 7. Model sensitivity to the maximum considered frequency as obtained for example E2. Results shown at the upper row are based on the maximum frequency $f_{max} = 5f_p$ where f_p is the incoming frequency (similar results of Kaihatu and Kirby, 1995 were presented by Kim and Kaihatu, 2021, Fig. 6 and provide verification to the computation conducted here). Results shown at the lower row are based on $f_{max} = 8f_p$. These results can be also compared with the results shown in Fig. 5 for which $f_{max} = 6f_p$.
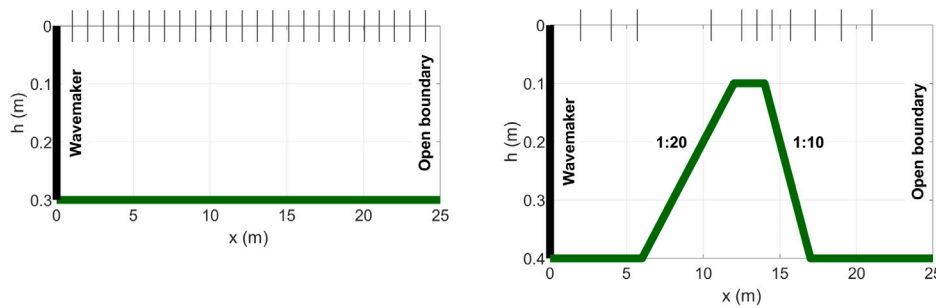

Fig. 8. Schematic illustration of the experiments conducted by Chapalain et al. (1992) (left panel) and Dingemans (1994) (right panel). The structures of the bathymetries are described by the thick green lines. The thin vertical lines, plotted along the still water level ($h = 0$), indicating measurement locations.

incoming wave conditions provide a challenging case for prediction, especially when the prediction is based on the quadratic formulation which neglects third and higher order terms.

The second example is an experiment conducted first by Beji and Battjes (1993) and later by Dingemans (1994), which describes monochromatic wave propagation over a submerged bar (see illustration in Fig. 8). Specifically, 'measuring condition A' (as referred to by Dingemans, 1994) is considered and detailed in Table 2. The evolution of the wave field being generated in this example involves several interesting phenomena, which are briefly described as follows. The wave adjacent to the wavemaker can be characterizes as a permanent second-order Stokes wave. Over the front slope of the bar the wave steepens, suggesting the development of higher harmonics. This process is accelerated over the head of the bar, where resonance due to triad interactions is nearly met. Ultimately, behind the bar, the increasing water depth decreases the effect of nonlinearity, and therefore, decouples the mutual forcing between the harmonics. As a consequence, this de-shoaling process results in completely different wave conditions than the incoming conditions (compare the incoming and outgoing amplitudes presented by the panels in Fig. 10). This combination of phenomena results from the interplay of nonlinearity and dispersion. The fact that in this example the roles of both of these wave properties are important makes this example a standard test case for wave model verification.

The parameters detailed in Table 2 indicate that both of the examples describe wave evolution in relatively shallow water depth. Note the distinction between the Ursell number of the incoming wave and the maximum Ursell number. The latter is estimated based on linear shoaling of the incoming monochromatic component. The relatively

high U_r value that characterizes the case of Chapalain et al. (1992) indicates on significant energy exchanges between wave harmonics along the entire flume. The second case of Dingemans (1994) also presents high values of U_r, but these are limited only to short segment of the domain. Specifically, U_r of the second case is higher than the validity limit of the second-order Stokes expansion ($U_r = 26$) over the region $10.5 \le x \le 14.8$, reaching to a very high value ($U_{r,max}$) at the top of the bar.

These examples are computed with the different quadratic formulations using the first six harmonics for the case of Chapalain et al. (1992) and using the first eight harmonics for the case of Dingemans (1994) (the first harmonic serves as the frequency step and the maximum frequency is the sixth or the eighth harmonic). The comparison between the different quadratic models and the measurements is discussed in the following.

5.1.1. Monochromatic wave evolution over constant depth

The predictions of the different quadratic formulations for the case of Chapalain et al. (1992) are compared to laboratory observations in Fig. 9. As expected, the high value of U_r leads to significant energy exchanges between the harmonics, such that the amplitudes of the first and the second harmonics become approximately equal to each other at certain locations. The predictive capabilities of the models are measured here with respect to the magnitude of the amplitudes and the beat lengths. Generally speaking, the Boussinesq models tend to underestimate the magnitude of the amplitudes, while the fully dispersive models tend to overestimate those magnitudes. Additionally, most of the predictions show some discrepancies of the beat lengths with respect to the measurements. Clearly, the deviations in the predictions

Table 2

Incoming wave parameters (indicated by the subscript 'I') and maximum Ursell number ($U_{r,max}$) of the considered monochromatic examples.

Example	T (s)	μ_I	amp_I (m)	$U_{r,I}$	$U_{r,max}$
Chapalain et al. (1992) (Trial D)	2.5	0.454	0.0354	45.2	45.2
Dingemans (1994) (Condition A)	2.02	0.67	0.01	4.5	101.5
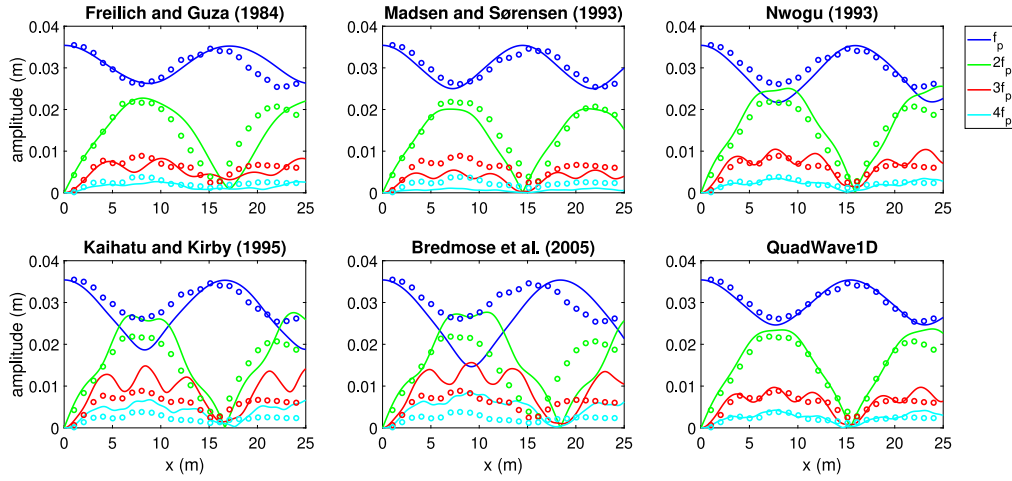
Fig. 9. Amplitude evolution of the first four harmonics as obtained by the different quadratic formulations (lines) and the laboratory results measured by Chapalain et al. (1992) (circles).
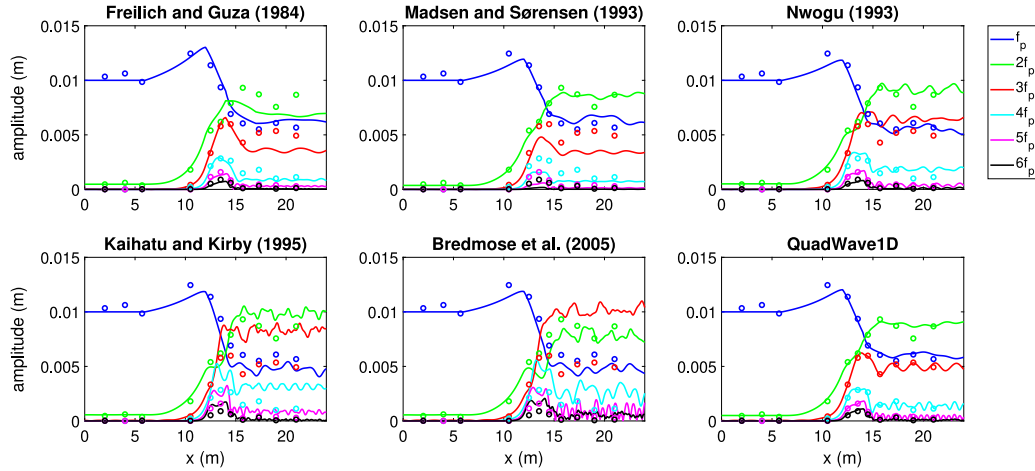
Fig. 10. Amplitude evolution of the first six harmonics as obtained by the different quadratic formulations (lines) and the laboratory results measured by Dingemans (1994) (circles).

are much more pronounced by the model results of the fully dispersive formulations. In part, these pronounced deviations are also attributed to the unfavourable behaviour of these models in the presence of very high frequencies (as briefly discussed in Section 4.2). The exceptional results are those of Nwogu (1993) and QuadWave1D. These model predictions show good agreement with the laboratory observations in terms of both amplitude values and beat lengths (see also model performance metrics in Appendix B, Table 5). Note however that the results due to Nwogu (1993) slightly overpredicts the energy transfer between the harmonics, leading to more obvious deviations than those obtained through QuadWave1D.

5.1.2. Monochromatic wave evolution over a bar

The evolution of monochromatic wave over a bar is described by the different quadratic formulations in Fig. 10. Generally speaking, the comparison of the computed and measured results suggests that all the formulations capture the expected physical phenomena emerging

in this example. Namely, the permanent Stokes behaviour over the incoming zone, the harmonics' growth over the bar and the decoupling of the harmonics in deeper water beyond the bar where they are essentially propagate as linear waves (this process effectively decomposes the initial wave into its harmonics, as nicely described by Beji and Battjes, 1993). However, the main modelling challenge of this example is to correctly describe the development of the harmonics outside the validity range of second-order Stokes theory, i.e., over the region $10.5 \leq x \leq 14.8$. As shown in Fig. 10, the fully dispersive models describe excessive energy exchanges between the harmonics and thus inaccurately describe the development of the different amplitudes. As a result, these models mispredict the output spectrum. In addition, these models also describe rapid oscillations attributed to the sensitivity of these models to the presence of very high frequencies (here $f_{max} = 8f_p$ is used, while slightly better predictions of these models are obtained when using $f_{max} = 6f_p$). The predictions of the Boussinesq models, on the other hand, seem much more adequate and show better agreement with the measurements. Nevertheless, some
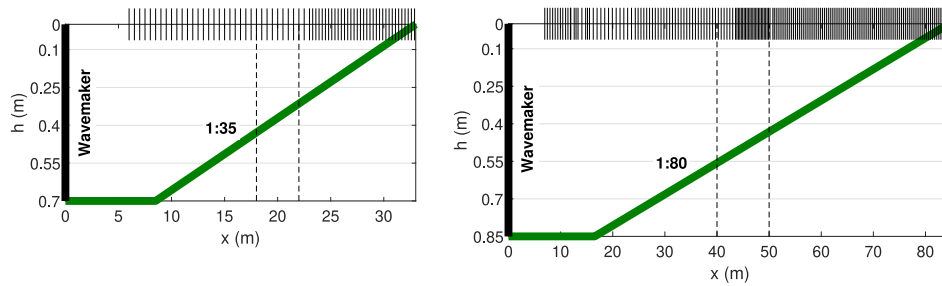
Fig. 11. Schematic illustration of the experiments conducted by Van Noorloos (2003) (left panel) and Ruessink et al. (2013) (right panel). The structures of the bathymetries are described by the thick green lines. The thin vertical lines, plotted along the still water level ($h = 0$), indicating measurement locations. The vertical dashed lines indicate the locations where computed and measured wave spectra are compared.

deviations are demonstrated by these predictions as well, given by the underprediction of Freilich and Guza (1984) and Madsen and Sørensen (1993) and overprediction of Nwogu (1993). Finally, QuadWave1D demonstrates the most adequate results and accurately agrees with the measurements. These findings are also supported by the model performance metrics detailed in Appendix B, Table 6.

To summarize, the two examples considered here provide satisfying verification for the modelling capabilities of QuadWave1D to describe the development of a monochromatic wave under significant nonlinear conditions and under conditions that combine nonlinearity, dispersion and bathymetry changes. The Boussinesq models also show satisfactory predictions, demonstrating only limited deviations in comparison with the measurements. However, the deviations observed through the fully dispersive models are significant. The unfavourable behaviour of these models requires further investigation which is beyond the scope of the present study. It seems though that these formulations are sensitivity to the presence of very high frequencies, which creates uncertainty regarding the choice of the maximum frequency considered, and thus, limiting the capabilities of these models to provide reliable predictions.

5.2. Evolution of bichromatic groups and irregular waves over a slope

The predictive capabilities of Quadwave1D are further investigated for more general cases involving multi-component wave fields. Specifically, two sets of laboratory experiments conducted by Van Noorloos (2003) and Ruessink et al. (2013) are considered. Generally speaking, these experiments describe one-dimensional, nonlinear shoaling of wave fields over a mild slope. The settings of these experiments are described schematically in Fig. 11 and the parameters of the incoming wave fields are detailed in Tables 3 and 4. Model capabilities are examined by comparisons to measured results and to the predictions of SWASH up to the breaking points beyond which the quadratic formulations become invalid. The comparison focuses on the evolution of the primary components and the generation and development of the secondary components (the super and sub harmonics). Special attention is devoted to the modelling performance of the different quadratic formulations to predict the generation and growth of the subharmonics (the infragravity components). Finally, recall that the quadratic formulations only account for the incoming wave components. Therefore, the examined cases considered here are such that the effect of wave reflection on the evolution of the primary and secondary components is negligible (see results by Rijnsdorp et al., 2014 and De Bakker et al., 2015). Accordingly, the measured data is not separated into incoming and reflected wave components. Nevertheless, the simulations conducted with SWASH attempt to avoid the contribution of the reflected part. This is performed by applying a radiation condition on the down-wave side of the domain at a depth of $h \sim 0.057$ m accompanied by a sponge layer of 5 m in front of it. The combination of these measures allows an effective absorption of both the long and the short wave components, as verified in Figs. 12 and 15.

5.2.1. Bichromatic groups over a slope

Three bichromatic examples introduced by Van Noorloos (2003) (i.e., A1, B3 and B5) are considered. Wave predictions for these examples as obtained by the different quadratic formulations are compared to measured and SWASH results in Fig. 12. The comparison is presented in terms of the H_s of the primary and super harmonics (defined by $f > f_{ig,max}$ and referred to as the sea-swell components) and the H_s of the sub harmonics (defined by $f \leq f_{ig,max}$ and referred to as the infragravity (IG) components), where the separating frequency takes the following value: $f_{ig,max} = 0.3$ Hz. Additionally, the results using the quadratic approach are computed through spectral resolution of $\Delta f = 0.025$ Hz and maximum frequency of $f_{max} = 4f_p$ (recall that f_p is the peak frequency). Furthermore, these results use an ensemble average of 10 realizations. Finally, the results according to SWASH are time-averaged over the last 6 min, where the total simulation time is chosen to be 10 min.

The values given in Table 3 indicate that the considered examples describe incoming wave groups over intermediate water depth. Additionally, these groups are characterized by relatively small incoming U_r value (see $U_{r,I}$ in Table 3). Therefore, it is expected that wave evolution up to $x \sim 10$ would agree with the second-order permanent Stokes solution. In fact, the Ursell number only becomes significant around the breaking area. Thus, the evolution is expected to be quasi-linear, namely, dominated by linear dispersion and shoaling along most of the domain (up to $x \sim x_{s,max}$) for all the considered examples. Based on these expectations, the predictions presented by the fully dispersive models are surprising. These predictions describe significant energy transfers from the primary component (i.e., the component with frequency f_3) to secondary components, as implied by the decrease of the sea-swell H_s and the relatively rapid H_s growth of the IG components. The mechanism which triggers these energy exchanges is attributed to modulational instability, as explained by Akrish et al. (2024).

On the other hand, the Boussinesq formulations agree better with the measured and SWASH results and with the expectation of quasi-linear evolution. Nevertheless, exceptional Boussinesq results are described by the predictions of Freilich and Guza (1984) and Madsen and Sørensen (1993). The former overpredicts the sea-swell H_s due to an overestimation of the linear shoaling (as a consequence of the weak dispersion assumption). Whereas the latter overpredicts the infragravity H_s as a result of the nonlinear balance generated by the quadratic coefficients, $V_{l,m}$, which is characterized by relatively strong tendency towards sub interactions (as also described by the bound wave solutions of Madsen and Sørensen, 1993, see Akrish et al., 2024, Fig. 1). In summary, it seems that the model by Nwogu (1993) and QuadWave1D describe most adequately the development of the wave groups for the considered examples (similar conclusion can also be drawn based on the model performance metrics given by Appendix B, Table 7). These adequate predictions are obtained due to a combination of accurate linear formulation (dispersion and shoaling) and adequate nonlinear balance provided by the quadratic coefficients.

Table 3

Incoming wave parameters for the bichromatic examples of Van Noorloos (2003). The incoming forced amplitude amp_1 of the sub harmonic indicated by f_1 is calculated based on second-order Stokes theory. Additionally, $U_{r,max}$ estimates the Ursell number at the breaking point and $x_{s,max}$ estimates the maximum location for which $U_r < 26$.

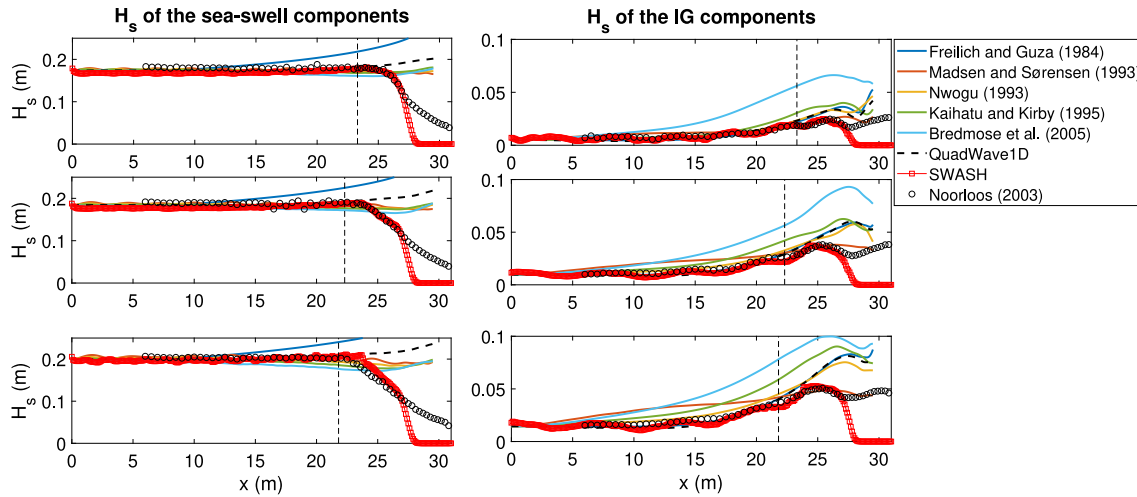| Exp.	f_3 (Hz)	f_2 (Hz)	f_1 (Hz)	amp_3 (m)	amp_2 (m)	μ_I	$U_{r,I}$	$U_{r,max}$	$x_{s,max}$ (m)
A1	0.6714	0.4761	0.1953	0.06	0.012	1.43	4.7	41.8	21
B3	0.6470	0.5005	0.1465	0.06	0.024	1.35	5.6	39.2	20
B5	0.6470	0.5005	0.1465	0.06	0.036	1.35	6.0	38.6	19

Fig. 12. A comparison of computed and measured H_s for the bichromatic examples A1 (upper row), B3 (middle row) and B5 (lower row) of Van Noorloos (2003). The vertical dashed lines provide estimation for the wave breaking locations.
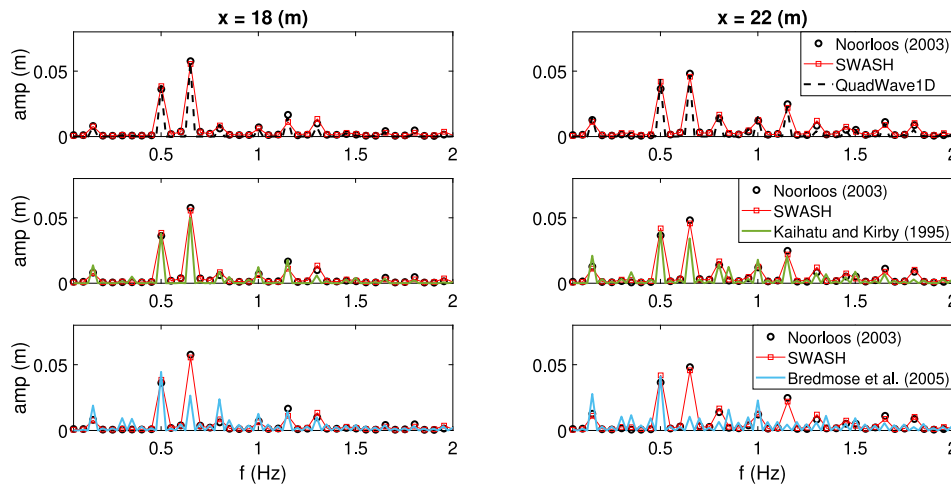

Fig. 13. A comparison of amplitude spectra as obtained by the measurements, SWASH and the fully dispersive models.

The prediction capabilities of QuadWave1D in comparison to the other quadratic formulations is further investigated using example B5, which describes the most significant incoming wave conditions in terms of nonlinearity. Further insight is gained by considering the predicted spectral development of the group along the flume. To this end, Figs. 13–14 present the amplitude spectra at two different locations in the vicinity of the breaking point. This spectral point of view provides further evidence to the impact of modulational instability on the evolution of the wave group. Especially, the results of Bredmose et al. (2005), but also less prominently the results of Kaihatu and Kirby (1995), show significant energy transfer from the primary component to the side-bands, providing explanation to the amplitude increase of the modulation frequency (as apparent in Fig. 13 at $x = 18$ m). This initial stage is followed by a significant spectrum broadening towards sub and super harmonics (as presented in Fig. 13 at $x = 22$ m). The

predictions of the rest of the models agree well with the measured and SWASH results. Especially, the results of Freilich and Guza (1984) and Nwogu (1993) and QuadWave1D show accurate development of the complete spectrum. The prediction of Madsen and Sørensen (1993) though, tend to underpredict the development of the super harmonics (as also demonstrated earlier for the monochromatic cases).

5.2.2. Irregular waves over a slope

The last verification examples of QuadWave1D are devoted to the evolution of irregular wave fields. The considered examples are the irregular cases which were experimentally investigated by Ruessink et al. (2013). The choice of these examples is motivated by the relatively shallow water and mild slope conditions that characterize them. Under these conditions, nonlinear wave transformation occurs over a relatively long domain (compared to conditions characterized by
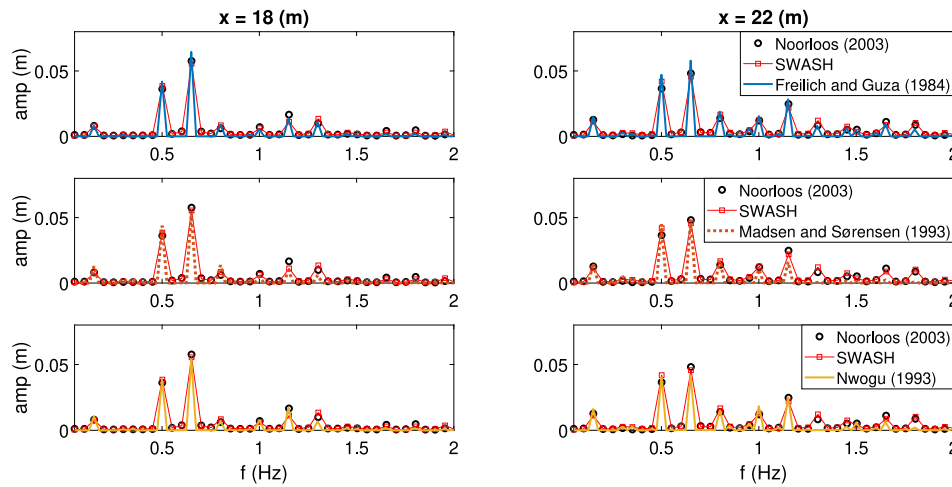
Fig. 14. A comparison of amplitude spectra as obtained by the measurements, SWASH and the Boussinesq models.

Table 4

Wave parameters for the irregular examples of Ruessink et al. (2013). The incoming wave fields are defined based on the JONSWAP spectrum requiring the values of f_p, H_s and γ (γ stands for the peak-enhancement factor). Also here, $U_{r,max}$ represents the Ursell number at the breaking point and $x_{s,max}$ indicates the maximum location for which $U_r < 26$.

Exp.	f_p (Hz)	H_s (m)	γ	$f_{ig,max}$	μ_I	$U_{r,I}$	$U_{r,max}$	$x_{s,max}$ (m)
A1	0.6329	0.1	3.3	0.37	1.5	2.1	47.5	61
A2	0.4444	0.2	3.3	0.26	0.9	11.4	52.5	37
A3	0.4444	0.1	20	0.26	0.9	5.7	77.3	49

relatively steep slopes for which the nonlinear transformation is quite local) and is governed by the quadratic term. Consequently, these conditions allow to highlight the predictive capabilities of the different quadratic formulations to describe the nonlinear development of the sea-swell components and the associated infragravity response over depths that characterize the coastal environment.

The generated wave fields for these examples are defined based on the JONSWAP spectrum using the parameters detailed in Table 4. The computations through the quadratic formulations are based on a spectral resolution of $\Delta f = 0.015$ Hz, maximum frequency of $f_{max} = 4f_p$ and averaging over 60 realizations. The computations through SWASH is based on a simulation time of 60 min, where the results presented are time-averaged over the last 54 min.

The computed and measured results are compared in Fig. 15 in terms of H_s. Here again, the values of H_s are presented separately for the shorter waves (denoted as the sea-swell components and satisfy $f > f_{ig,max}$) and for the longer waves (denoted as the infragravity (IG) components and satisfy $f \leq f_{ig,max}$), where the separation frequency, $f_{ig,max}$, is provided in Table 4 for each of the considered examples. For the intermediate to shallow water depth conditions that characterize these examples, the values of $x_{s,max}$ define the regions over which second-order Stokes theory is expected to be valid. Over these regions, wave evolution is expected to be dominated by linear dispersion and shoaling, while evidence of nonlinear exchanges of energy is expected to be weak. This highlights again the abnormal infragravity responses shown by the fully dispersive formulations in Fig. 15. These results are explained by the spurious impact of modulational instability, as discussed in detail by Akrish et al. (2024). Furthermore, the results of Fig. 15 provides an additional evidence to the reliability of wave prediction using QuadWave1D and the Boussinesq models for water depths which characterize the coastal environment. These models agree well with the measured and SWASH results up until the breaking points. However, also here, the inaccurate shoaling prediction of Freilich and Guza (1984) and the inadequate nonlinear balance due to the quadratic

coefficients of Madsen and Sørensen (1993) result in overprediction of the sea-swell H_s and the infragravity H_s, respectively.

Further details explaining the prediction capabilities of QuadWave1D in comparison to other quadratic formulations are presented in Figs. 16–17. These results provide a limited view on the spectral evolution as obtained for example A2 close to the breaking point. In order to highlight the modelling capabilities of the infragravity components, the spectra are plotted through logarithmic scales. The results provide another perspective on the effect of modulational instability, which induces much faster spectral broadening than predicted by the measurements (especially notable by the results of Bredmose et al., 2005, but also seen less obviously through the results of Kaihatu and Kirby, 1995, as presented in Fig. 16). In addition, the tendency of the model by Madsen and Sørensen (1993) to overpredict the subharmonic responses and to underpredict the superharmonic responses is revealed again through Fig. 17. In summary, QuadWave1D and the model by Nwogu (1993) seems to generate the most accurate prediction for this example, as also suggested by the model performance metrics presented in Appendix B, Table 8.

To summarize, the verification conducted for both bichromatic an irregular wave conditions shows the preferable prediction capabilities of QuadWave1D and the Boussinesq models. However, all the examples considered showed the tendency of Freilich and Guza (1984) to overpredict the sea-swell components due to inaccurate formulation of linear shoaling and the tendency of Madsen and Sørensen (1993) to underpredict the sea-swell components and to overpredict the IG components due to inadequate nonlinear balance provided by the quadratic coefficients. QuadWave1D and the model of Nwogu (1993) present the most satisfying general agreement with the measured and SWASH results, and together with the model of Freilich and Guza (1984) showed the most accurate prediction of the infragravity response (see also the results of the performance metrics in Tables 7–8, which provide additional support to this conclusion). Finally, as observed for the monochromatic cases, also here the predictions of the fully dispersive formulations deviated considerably from the measurement results. However here, the observed deviations are explained by Akrish et al. (2024) to arise due to false impact of the modulational instability mechanism.

Ultimately, the model verification presented along this section demonstrates the accuracy of QuadWave1D to predict the nonlinear evolution of one-dimensional wave fields over coastal waters. Specifically, comparing to other quadratic formulations and based on a wide set of examples (including monochromatic, bichromatic and irregular wave conditions), it is found that QuadWave1D presents superior predictive capabilities of both the sea-swell components and the infragravity field.
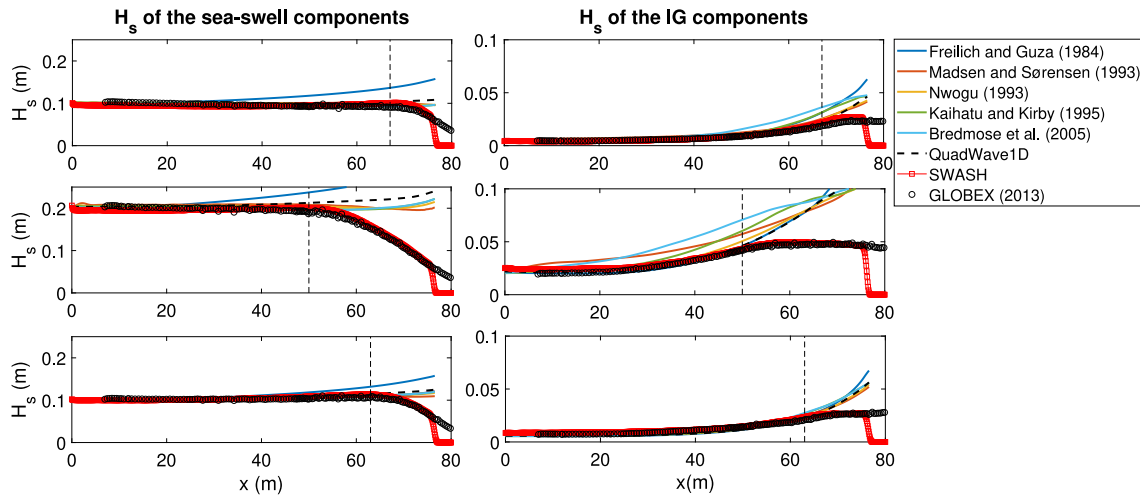
Fig. 15. A comparison of computed and measured H_s for the irregular examples A1 (upper row), A2 (middle row) and A3 (lower row) of Ruessink et al. (2013). The vertical dashed lines provide estimation for the wave breaking locations.
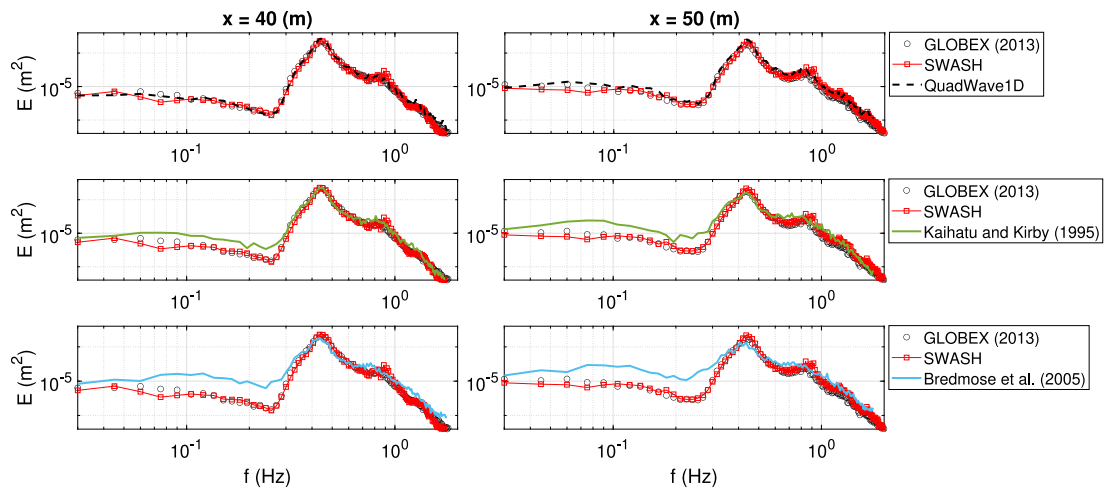

Fig. 16. A comparison of variance spectra as obtained by the measurements, SWASH and the fully dispersive models.
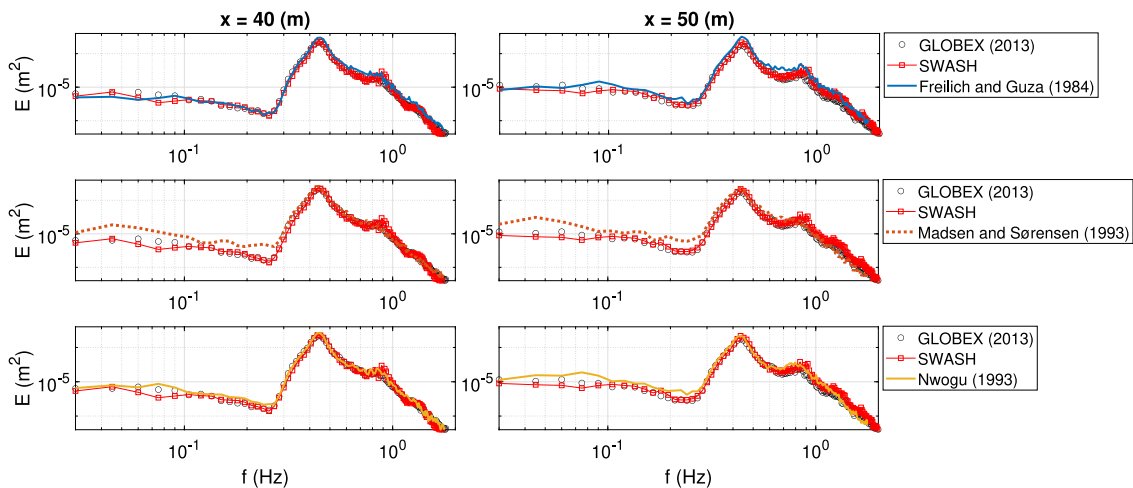

Fig. 17. A comparison of variance spectra as obtained by the measurements, SWASH and the Boussinesq models.

6. Discussion and concluding remarks

This study presents an attempt to find the quadratic formulation that describes most adequately nonlinear wave developments over water depths and bathymetrical structures that characterize the coastal environment. To this end, an optimization process was proposed to search for the quadratic formulation that minimize evolution errors comparing to experimental data and data obtained based on the SWASH model (Zijlema et al., 2011). The outcome is the model QuadWave1D: a fully dispersive quadratic model for coastal wave prediction in one-dimension.

The validation study of QuadWave1D consisted of different cases involving different incoming wave conditions and bottom topographies. Based on the considered examples and comparing to other quadratic formulations, it is found that QuadWave1D presents superior predictive capabilities of both the sea-swell components and the infragravity field.

Interestingly, the satisfying predictive capabilities of QuadWave1D seem to consistently hold for examples with significant bathymetrical changes despite the fact that it was formulated based on constant depth conditions. This finding supports the commonly used assumption (which is taken here as well) that the linear shoaling term is typically of the same order as the quadratic nonlinear term, and therefore, the contributions of the two can be analysed independently.

Although seem promising, the predictive capabilities of QuadWave1D are limited. Some limitations arise due to the definition of its quadratic coefficients (the so-called Weighted Quadratic Coefficients). Generally speaking, this definition is based on two types of requirements: the formal type (e.g., full dispersion, conservative triad interactions, etc.) and the heuristic type which further constraint the search of suitable coefficients. The additional constraints created by the latter led to the choice of a specific functional structure for the quadratic coefficients of QuadWave1D. As a consequence, the original optimization problem was reduced to a much simpler problem of finding only three unknowns (i.e., α_1, α_2 and α_3). Despite the resulting convenience, reducing the problem also limits the search space, and consequently, limits the accuracy of the optimal result in comparison with the solution of the original problem. For example, modifications of the heuristic requirements and of the representative functional structure would inevitably lead to a different definition of the quadratic coefficients and may even improve the prediction accuracy comparing to QuadWave1D.

Despite the doubts concerning the use of the heuristic requirements, it seems that the heuristic requirement (also implemented by Quad-Wave1D) to limit the values of the interaction coefficients that involve high frequencies is essential for reliable prediction of coastal waves. This requirement is based on the experience gained working with fully dispersive formulations for which such interaction coefficients tent to be high valued and lead to the emergence of unfavourable and unexpected energy exchanges (partially explained in Akrish et al., 2024 through the impact of modulational instability). Note, however, that this requirement also dictates a trade-off between reliable prediction of wave evolution over shallower waters and known nonlinear wave properties over deeper water (e.g., bound wave solutions and amplitude dispersion). Consequently, QuadWave1D which is based on this heuristic requirement would not be suitable to describe wave nonlinearity in deep water. Additionally, as applies to other quadratic models, QuadWave1D cannot describe wave reflection and the development of standing wave patterns in front of structures. For problems involving such phenomena, QuadWave1D should be coupled with a different type of model. However, as considered for other quadratic formulations in the past (e.g., Kaihatu and Kirby, 1995 and Kim and Kaihatu, 2021), QuadWave1D can be potentially generalized to allow for wave breaking and directional wave propagation over two-dimensional bottom topography. Finally, it should be noted that apart from being a stand-alone model, QuadWave1D also serves as a reliable and accurate starting point for the stochastic formulation of shallow water nonlinearity. As such, QuadWave1D provides an opportunity to improve the nonlinear source term (i.e., S_{nl3}) that is currently implemented in spectral models.

CRediT authorship contribution statement

Gal Akrish: Writing – original draft, Validation, Software, Methodology, Formal analysis, Conceptualization. **Ad Reniers:** Writing – review & editing, Supervision, Conceptualization. **Marcel Zijlema:** Writing – review & editing, Supervision. **Pieter Smit:** Writing – review & editing, Supervision.

Declaration of competing interest

The authors declare that they have no known competing financial interests or personal relationships that could have appeared to influence the work reported in this paper.

Data availability

Data will be made available on request.

Acknowledgements

Appendix A. The quadratic coefficients of QuadWave1D

QuadWave1D is a fully dispersive quadratic model defined with the following parameterized quadratic coefficients:

$$V_{l,m}^{WQC} = W_{l,m} V_{l,m}^{BC} \qquad (19)$$

Recall that WQC and BC stand for 'Weighted Quadratic Coefficients' and 'Bredmose Coefficients', respectively. The weight function, $W_{l,m}$, is defined by (13) and (14) and using the coefficient values $\alpha_1 = 1$, $\alpha_2 = 1.4$, $\alpha_3 = 5.5$. The quadratic coefficients $V_{l,m}^{BC}$ were introduced by Bredmose et al. (2005) and can be written as follows (see further details by Akrish et al., 2024, Supplementary material):

$$V_{l,m} = -N_{l,m}/H_{lm} \qquad (20)$$

where $N_{l,m}$ and H_{lm} are defined as

$$N_{l,m} = -\frac{1}{2}\frac{g}{\omega_l \omega_m}\left(\omega_{lm}^2 k_l k_m + \omega_n k_{lm}(k_l \omega_m + k_m \omega_l)\right)$$
$$-\frac{1}{2}\frac{\omega_n^2}{g}\left(\frac{\omega_{lm}^2}{\omega_n^2}\omega_l \omega_m - \omega_{lm}^2\right) \qquad (21)$$

$$H_{lm} = \frac{\omega_n^2 - \omega_{lm}^2}{k_n - k_{lm}} \qquad (22)$$

and k_{lm} and ω_{lm}^2 are given by

$$k_{lm} = k_l + k_m \qquad (23)$$

$$\omega_{lm}^2 = k_{lm} g \tanh(k_{lm}h). \qquad (24)$$

Appendix B. Model performance metrics

This appendix provides a quantitative comparison of the results presented in Section 5. Specifically, the results detailed here aim to provide additional formal indication to the predictive capabilities of the different model formulations, which have so far been presented only visually. To this end, formal metrics are defined to determine model performance for the two monochromatic examples of Chapalain et al. (1992) and Dingemans (1994), and for the more general B5 and A1 examples of Van Noorloos (2003) and Ruessink et al. (2013),

Table 5
Model errors for the monochromatic example of Chapalain et al. (1992), calculated for each frequency as a sum over the available measurement points.

Frequency	FG84	MS93	N93	KK95	B05	QW1D
f_p	1.045	0.887	1.387	2.014	3.464	**0.585**
$2f_p$	1.937	1.316	1.722	2.424	4.043	**0.975**
$3f_p$	0.901	1.573	0.886	2.348	3.214	**0.795**
$4f_p$	0.516	1.084	**0.341**	1.317	2.016	0.380

Table 6
Model errors for the monochromatic example of Dingemans (1994), calculated for each frequency as a sum over the available measurement points.

Frequency	FG84	MS93	N93	KK95	B05	QW1D
f_p	0.567	0.572	0.518	1.069	0.978	**0.362**
$2f_p$	0.818	**0.247**	0.381	0.748	0.948	**0.247**
$3f_p$	0.547	0.987	0.808	1.782	2.580	**0.077**
$4f_p$	0.298	0.635	0.307	1.197	1.028	**0.122**
$5f_p$	**0.090**	0.345	0.153	0.372	0.713	0.129
$6f_p$	0.123	0.232	0.095	0.224	0.474	**0.057**

Table 7
Model errors for example B5 of Van Noorloos (2003), calculated as a sum over the points $x = 12$ (m), $x = 18$ (m) and $x = 22$ (m) and a sum over the specified frequency band.

Frequency band	FG84	MS93	N93	KK95	B05	QW1D	SWASH
Infragravity ($0.05 \leq f \leq 0.30$)	0.513	0.729	0.462	0.633	1.291	**0.454**	**0.211**
Sea-Swell ($0.30 < f \leq 2.25$)	1.612	1.863	1.579	1.517	3.579	**1.239**	**0.768**

Table 8
Model errors for example A2 of Ruessink et al. (2013), calculated as a sum over the points $x = 30$ (m), $x = 40$ (m) and $x = 50$ (m) and a sum over the specified frequency band.

Frequency band	FG84	MS93	N93	KK95	B05	QW1D	SWASH
Infragravity ($0.015 \leq f \leq 0.26$)	0.179	0.586	0.220	0.503	0.997	**0.153**	**0.157**
Sea-Swell ($0.26 < f \leq 1.755$)	2.549	1.567	**1.193**	1.556	2.504	1.526	**1.237**

respectively. The performance metrics used here are based on the error definition given by (17), which for convenience, is rewritten as

$$e = \sum_j \sum_i |amp_{i,j} - amp_{R,i,j}|/amp_I \qquad (25)$$

where j runs over the desired wave frequencies and i runs over the data locations. Recall that $amp_{i,j}$ and $amp_{R,i,j}$ represent the amplitude results as given by the model prediction and by the measurements, respectively. Finally, amp_I indicates the incoming amplitude, which is defined by the amplitude of the primary frequency (i.e., f_p) for the monochromatic cases or by $H_s/2$ for the more general cases.

To ease the presentation, the different model formulations are referred to here using the first letter of their developers and the last two digits of their publication year (e.g., the model by Freilich and Guza, 1984 is referred to as FG84). The only exception is the model by Bredmose et al. (2005) which is referred to only based on the first author (i.e., B05). Finally, QuadWave1D is referred to here as QW1D.

The model errors for the monochromatic cases are detailed in Tables 5–6. The errors are defined for each harmonic separately. Namely, these errors are calculated through (25), as a sum over i locations for each of the considered j. On the other hand, the model errors obtained for the more general cases in Tables 7–8 are defined for a frequency range, and therefore, defined as a sum over i and as a sum over the specified frequency band (specified by the first column of the tables).

References

Agnon, Y., Sheremet, A., Gonsalves, J., Stiassnie, M., 1993. Nonlinear evolution of a unidirectional shoaling wave field. Coast. Eng. 20 (1–2), 29–58.

Akrish, G., Reniers, A., Zijlema, M., Smit, P., 2024. The impact of modulational instability on coastal wave forecasting using quadratic models. Coast. Eng. 104502.

Ardani, S., Kaihatu, J.M., 2019. Evolution of high frequency waves in shoaling and breaking wave spectra. Phys. Fluids 31 (8), 087102.

Beji, S., Battjes, J., 1993. Experimental investigation of wave propagation over a bar. Coast. Eng. 19 (1–2), 151–162.

Booij, N., Ris, R.C., Holthuijsen, L.H., 1999. A third-generation wave model for coastal regions: 1. Model description and validation. J. Geophys. Res.: Oceans 104 (C4), 7649–7666.

Bowen, A.J., 1969. Rip currents: 1. Theoretical investigations. J. Geophys. Res. 74 (23), 5467–5478.

Bredmose, H., Agnon, Y., Madsen, P.A., Schäffer, H.A., 2005. Wave transformation models with exact second-order transfer. Eur. J. Mech.-B/Fluids 24 (6), 659–682.

Bredmose, H., Schäffer, H.A., Madsen, P.A., 2004. Boussinesq evolution equations: Numerical efficiency, breaking and amplitude dispersion. Coast. Eng. 51 (11–12), 1117–1142.

Chapalain, G., Cointe, R., Temperville, A., 1992. Observed and modeled resonantly interacting progressive water-waves. Coast. Eng. 16 (3), 267–300.

Craik, A.D.D., 1985. Wave Interactions and Fluid Flows. Cambridge University Press.

Dalzell, J., 1999. A note on finite depth second-order wave–wave interactions. Appl. Ocean Res. 21 (3), 105–111.

De Bakker, A., Herbers, T., Smit, P., Tissier, M., Ruessink, B.G., 2015. Nonlinear infragravity–wave interactions on a gently sloping laboratory beach. J. Phys. Oceanogr. 45 (2), 589–605.

Dingemans, M.W., 1994. Comparison of Computations with Boussinesq-Like Models and Laboratory Measurements. Memo in framework of MAST project (G8-M), Delft Hydraulics memo H1684. 12.

Dingemans, M.W., 1997. Water Wave Propagation over Uneven Bottoms, vol. 13, World Scientific.

Eldeberky, Y., 1996. Nonlinear Transformation of Wave Spectra in the Near-Shore Zone (Ph.D. thesis). Delft University of Technology.

Eldeberky, Y., Madsen, P.A., 1999. Deterministic and stochastic evolution equations for fully dispersive and weakly nonlinear waves. Coast. Eng. 38 (1), 1–24.

Fredsoe, J., Deigaard, R., 1992. Mechanics of Coastal Sediment Transport, vol. 3, World Scientific Publishing Company.

Freilich, M., Guza, R., 1984. Nonlinear effects on shoaling surface gravity waves. Philos. Trans. R. Soc. Lond. Ser. A 311 (1515), 1–41.

Hasselmann, K., 1962. On the non-linear energy transfer in a gravity-wave spectrum Part 1. General theory. J. Fluid Mech. 12 (4), 481–500.

Herbers, T., Burton, M., 1997. Nonlinear shoaling of directionally spread waves on a beach. J. Geophys. Res.: Oceans 102 (C9), 21101–21114.

Herbers, T., Russnogle, N., Elgar, S., 2000. Spectral energy balance of breaking waves within the surf zone. J. Phys. Oceanogr. 30 (11), 2723–2737.

Janssen, T., 2006. Nonlinear Surface Waves Over Topography (Ph.D. thesis). Delft University of Technology.

Kaihatu, J.M., 2001. Improvement of parabolic nonlinear dispersive wave model. J. Waterw. Port Coast. Ocean Eng. 127 (2), 113–121.

Kaihatu, J.M., Kirby, J.T., 1995. Nonlinear transformation of waves in finite water depth. Phys. Fluids 7 (8), 1903–1914.

Kim, I.-C., Kaihatu, J.M., 2021. A consistent nonlinear mild-slope equation model. Coast. Eng. 170, 104006.

Le Méhauté, B., 1976. An Introduction to Hydrodynamics and Water Waves. Springer Science & Business Media.

Lighthill, J., 2001. Waves in Fluids. Cambridge University Press.

Longuet-Higgins, M.S., 1970. Longshore currents generated by obliquely incident sea waves: 1. J. Geophys. Res. 75 (33), 6778–6789.

Madsen, P.A., Sørensen, O.R., 1992. A new form of the Boussinesq equations with improved linear dispersion characteristics. Part 2. A slowly-varying bathymetry. Coast. Eng. 18 (3–4), 183–204.

Madsen, P.A., Sørensen, O.R., 1993. Bound waves and triad interactions in shallow water. Ocean Eng. 20 (4), 359–388.

Mei, C.C., Stiassnie, M.A., Yue, D.K.-P., 2005. Theory and Applications of Ocean Surface Waves. World Scientific.

Nwogu, O., 1993. Alternative form of Boussinesq equations for nearshore wave propagation. J. Waterw. Port Coast. Ocean Eng. 119 (6), 618–638.

Peregrine, D.H., 1967. Long waves on a beach. J. Fluid Mech. 27 (4), 815–827.

Reniers, A., Battjes, J., 1997. A laboratory study of longshore currents over barred and non-barred beaches. Coast. Eng. 30 (1–2), 1–21.

Reniers, A., Zijlema, M., 2022. Swan surfbeat-1d. Coast. Eng. 172, 104068.

Rijnsdorp, D.P., Smit, P.B., Guza, R., 2022. A nonlinear, non-dispersive energy balance for surfzone waves: infragravity wave dynamics on a sloping beach. J. Fluid Mech. 944.

Rijnsdorp, D.P., Smit, P.B., Zijlema, M., 2014. Non-hydrostatic modelling of infragravity waves under laboratory conditions. Coast. Eng. 85, 30–42.

Roeber, V., Bricker, J.D., 2015. Destructive tsunami-like wave generated by surf beat over a coral reef during Typhoon haiyan. Nature Commun. 6 (1), 1–9.

Roelvink, D., Reniers, A., Van Dongeren, A., de Vries, J.v.T., McCall, R., Lescinski, J., 2009. Modelling storm impacts on beaches, dunes and barrier islands. Coast. Eng. 56 (11–12), 1133–1152.

Ruessink, B.G., Michallet, H., Bonneton, P., Mouazé, D., Lara, J., Silva, P.A., Wellens, P., 2013. Globex: wave dynamics on a gently sloping laboratory beach. In: Proceedings Coastal Dynamics. pp. 1351–1362.

Ruessink, B.G., Miles, J., Feddersen, F., Guza, R., Elgar, S., 2001. Modeling the alongshore current on barred beaches. J. Geophys. Res.: Oceans 106 (C10), 22451–22463.

Sharma, J., Dean, R., 1981. Second-order directional seas and associated wave forces. Soc. Pet. Eng. J. 21 (01), 129–140.

Sheremet, A., Davis, J.R., Tian, M., Hanson, J.L., Hathaway, K.K., 2016. TRIADS: A phase-resolving model for nonlinear shoaling of directional wave spectra. Ocean Model. 99, 60–74.

Shi, F., Kirby, J.T., Harris, J.C., Geiman, J.D., Grilli, S.T., 2012. A high-order adaptive time-stepping TVD solver for Boussinesq modeling of breaking waves and coastal inundation. Ocean Model. 43, 36–51.

Stuhlmeier, R., Stiassnie, M., 2021. Deterministic wave forecasting with the Zakharov equation. J. Fluid Mech. 913, A50.

Tolman, H.L., 1991. A third-generation model for wind waves on slowly varying, unsteady, and inhomogeneous depths and currents. J. Phys. Oceanogr. 21 (6), 782–797.

Van Noorloos, J.C., 2003. Energy Transfer Between Short Wave Groups and Bound Long Waves on a Plane Slope (MSc thesis). Delft University of Technology.

Van Rijn, L.C., 1993. Principles of Sediment Transport in Rivers, Estuaries and Coastal Seas, vol. 1006, Aqua Publications Amsterdam.

Vanneste, J., 2005. Wave interactions. In: Nonlinear Waves in Fluids: Recent Advances and Modern Applications. Springer, pp. 69–94.

Vellinga, P., 1982. Beach and dune erosion during storm surges. Coast. Eng. 6 (4), 361–387.

Whitham, G.B., 1974. Linear and Nonlinear Waves. John Wiley & Sons.

Zijlema, M., Stelling, G., Smit, P., 2011. SWASH: An operational public domain code for simulating wave fields and rapidly varied flows in coastal waters. Coast. Eng. 58 (10), 992–1012.